GeoConvention 2015
GEOSCIENCE
new horizons
Telus Convention Centre • 4-8 May 2015 • Calgary, AB Canada

Three Dimensional Attenuation Tomography from microseismicity

Frank J. Calixto, University of Alberta
calixtom@ualberta.ca
Mirko van der Baan, University of Alberta

Summary

Attenuation images are obtained from 6287 t-star spectral measurements of P-wave microseismic events in a mine setting. The resulting three-dimensional quality factor (Q) model reveals that most of the study region is characterized by low Q values or high attenuation (Q<25), probably caused by cavities and fractures due to mining activities. Q values between 25 and 50 show a high spatial correlation with the location of an ore deposit. Furthermore, high quality ore deposits correlate with Q values of about 45-50 whereas the low quality ore correlates with Q values of around 30. Q values of less than 10 correlate with the observed seismic cloud epicenters. These features were previously partially resolved by velocity tomography. Therefore a joint interpretation is very important in determining the lithological properties and physical state of both, the region containing the seismic epicenters and the region with the ore deposits. The same methodology is applicable to microseismic data recorded during hydraulic fracturing treatment and may give more insight into fracture density of hydrocarbon reservoirs.

Introduction

The seismic quality factor (or inverse of attenuation) can provide valuable information on the lithology, fracture orientation and fluid presence of a region. The usefulness of attenuation tomography is sometimes limited by the azimuthal and depth coverage of the seismic stations. However, in the present study we have the advantage to work with microseismic events recorded by a total of 28 geophones deployed in seven boreholes. This array gives us a remarkable vertical coverage suitable for three-dimensional attenuation tomography. Another advantage is the relatively short time of recording needed to obtain sufficient data to obtain good resolution in the inversion as compare to experiments in global seismology (e.g. Calixto et al, 2013, 2014) where sometimes years of recording are needed. A total of 488 microseismic events used in this study were recorded during January, 2011. Their epicenters were obtained using the hypoDD approach (Castellanos and Van der Baan, 2013). A total of 6287 waveforms with observable P-wave arrivals were selected for the processing. Barthwal and Van der Baan (2014) used double difference tomography to invert for P-wave velocities and found that the epicenter of the seismic events fell in a region characterized by a transition from high to low P-wave velocities. They also found that cross cuts around 450 m depth are imaged as a low velocity zone. Castellanos and van der Baan (2014) found that events were dynamically triggered by removal of mining debris through the shaft and tunnel network rather than blasting activities.

Method

First, we attempted to measure the quality factor using a spectral ratio technique (Bao et al; 2011) called the two-station method which has the advantage to rule out any source time function assumption. However, we found that the required source-receiver geometry greatly constrained our observations to very few specific paths, thereby making very difficult to obtain optimal ray-crossing for a tomographic

inversion. Another limiting issue was the low signal to noise ratio in most of the recorded signals which makes the spectral ratio method a less optimal method for quality factor measurements (Tonn, 1991). Thus, we decided to measure Q by estimating the parameter t* assuming whole path attenuation (equation 1, Eberhart-Phillips, 2002) and the Brune's source model (see equation 2). This allow us to incorporate a greater number of ray paths in the inversion as geometrical constrains are not required. t* can be challenging to estimate but this study presents a way to obtain robust t* measurements. t* represents the cumulative spatial effect of attenuation along the ray path (Preston, 2014; Der and Lees, 1985) and is commonly expressed as:

$$t^* = \int_{path} \frac{1}{Q(r)v(r)}\,dr = \int_{path} \frac{1}{Q(r)}\,dt \qquad (1)$$

where the integral is calculated along the ray path. $Q(r)$ and $v(r)$ are the quality factor and seismic velocity at a location r along the ray path. dt is the travel time of the ray along the infinitesimal length dr within the ray path.
The Brune´s source model is given by:

$$A(f) = 2\pi f \Omega_0 \frac{f_c^2}{(f_c^2+f^2)} \exp[-\pi f(t^*)] \qquad (2)$$

Equation (2) defines the spectral velocity amplitude ($A(f)$) measured at a given station as a function of frequency. Ω_0 represents the spectral level and f_c is the corner frequency.

t* is estimated by spectral fitting of equation (2). The data used are 3 component velocity seismograms recorded by 28 geophones deployed in 7 boreholes in a mine. The components are rotated to the radial direction and then Fourier transforms of the window containing the signal and of a window with only noise are computed. In order to obtain robust results, frequency-depending signal to noise ratios (S/N) were calculated and used later as a weighting parameter in the spectral fitting (Reine et al., 2012). S/N ratios below 2 were assigned a weight of zero.
The equation used in the spectral fitting is obtained by taking the natural logarithm and rearranging equation 2:

$$L\big(A(f)\big) - Ln(2\pi f) + Ln\left(1 + \frac{f^2}{f_c^2}\right) = Ln(\Omega_0) - \pi f t^* \qquad (3)$$

Where the left side is known for a given f_c. Equation 3 actually represents a set of equations for different values of frequencies (in our case between 10 and 250 Hz). This set of equations is solved for $Ln(\Omega_0)$ and t^*using a weighted LSQR approach. Unlike Eberhart-Phillips (2002), we have decided to pick f_c from the signal with highest S/N ratio as estimating f_c from the measurement with the lowest misfit was found to be unreliable. The reason is that in many cases, waveforms with high noise content can produce low misfit. Once f_c is estimated for a given event, it is used in all stations that recorded the event to find t^* for each specific source-receiver path. Finally, equation (1) is discretized and used to solve for a three-dimensional model of Q using a weighted LSQR approach with the average S/N ratios previously calculated.

Results

Figure 1 shows an example of how f_c is estimated for an event with S/N=665.2. The f_c that best fits the velocity spectra is 55 Hz. Figure 2 shows a histogram of the 488 f_c's calculated. Their distribution is non-homogeneous with as many as 40 events having a f_c between 140 and 150 Hz. Lower f_c's can be related with a higher seismic moment and bigger crack radius for tensile events (Eaton et al., 2014). Although no estimations of seismic moment were available during the course of this study, f_c can give us a first order estimation of event magnitude and crack radius. For example: a f_c of 51.8 Hz would be related with a Mw=1.13 and crack radius=10.0 m (Eaton et al., 2014).

Figure 3 and 4 shows the results of the attenuation tomography. Although the values of Q obtained in the region vary between 0 and 1500 (not shown here), the vast majority fall in the range 0-50. Precisely in that range is that we observe some interesting correlations with the ore body location and the seismicity. The seismic cloud between y=100-250 m and z=350-500 m in figure 3 falls in a region with Q<10. Q values close to 30 in figure 3 shows a spatial correlation with the location of the ore body (y=300-400, z=400-500). Interestingly, the seismicity in this part of the region occurs beneath the basement rock beneath the ore body. Figure 4 shows a map view of the results with Q in the range 0-50. The transition from Q=50 to Q=30 in figure 4 (x=50-200, y=300-400) correlates with a transition from high quality to low quality of the ore body.

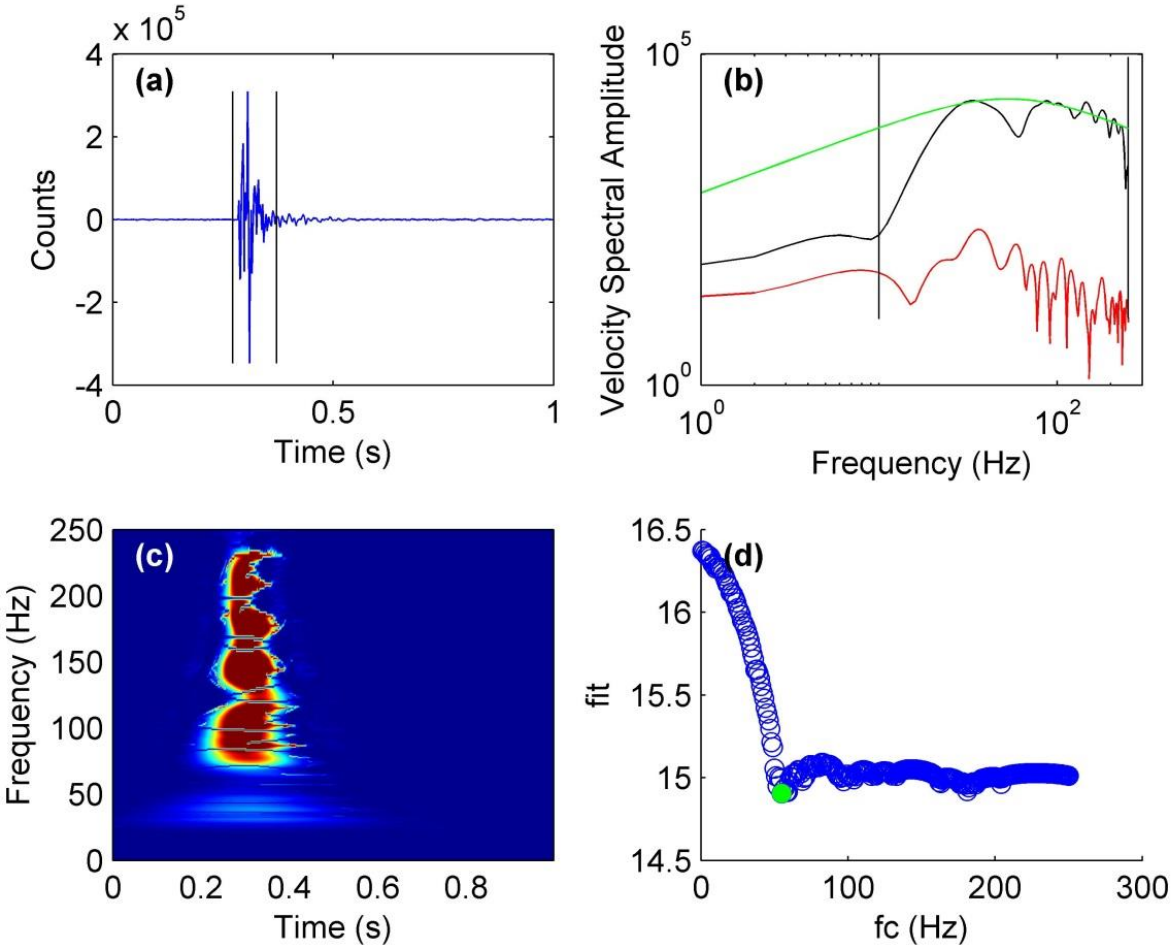

Figure 1: (a) Velocity seismogram of a microseismic event with S/N=665.2. The vertical bars denote the window used to calculate the velocity spectra. (b) Velocity spectra of a microseismic event (black curve) and noise (red curve). The green curve is the best fitting curve in the range 10-250 Hz. (c) Synchrosqueezing transform (Herrera et al., 2014) of (a) showing the P-wave frequency content in time roughly between 0.2 s and 0.4 s. (d) Misfit between the synthetic curve and the velocity spectral amplitude in (b) as f_c is grid-searched. Best fit is attained at 55 Hz corner frequency in this particular example (green dot) which is used to calculate the green curve in (b).

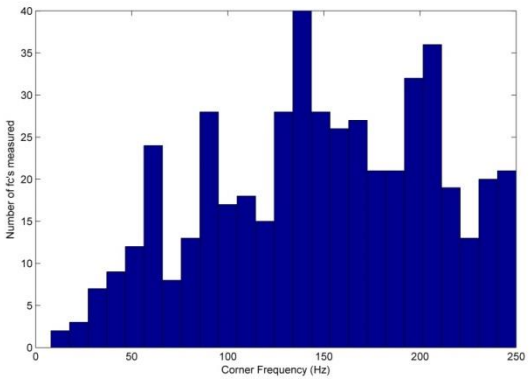

Figure 2: Histogram of the 488 corner frequencies estimated using grid search. Most of the corner frequencies are higher than 130 Hz.

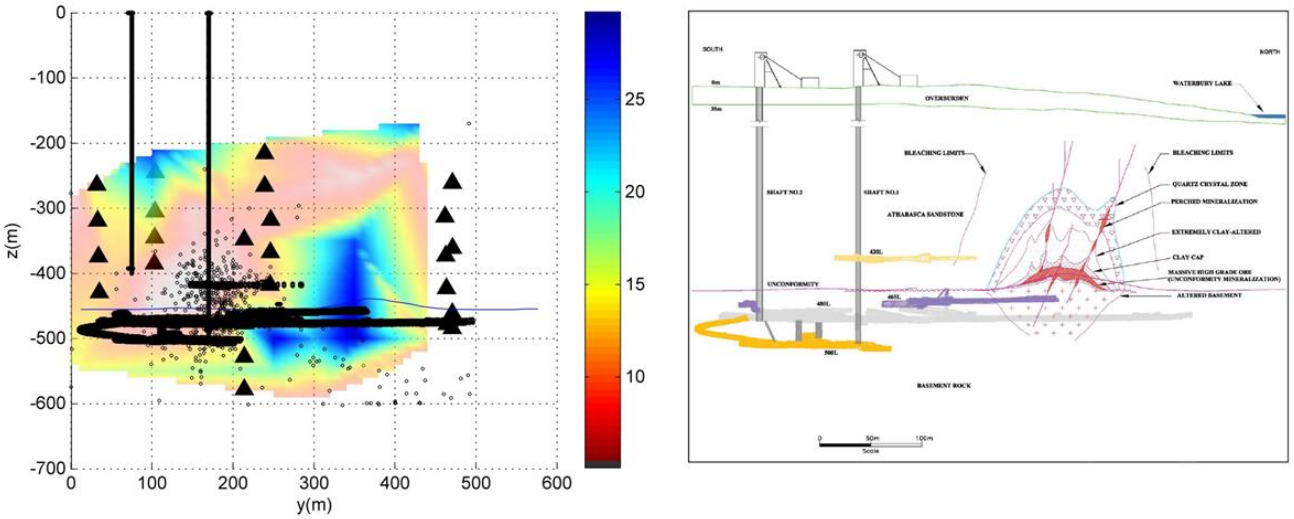

Figure 3: (Left) Q model cross section along the x=100 m with values in the range 0-30. The values of Q close to 30 highly correlated with the location of an ore deposit. Q values lower than 10 correlate with the location of the microseismic cloud. Black triangles represent the geophones. Black curves represent the tunnels and shafts. Black circles denote the hypocenters (from Castellanos and van der Baan, 2014). (Right) Uranium mine schematic cross-section illustrating the shape of the deposit.

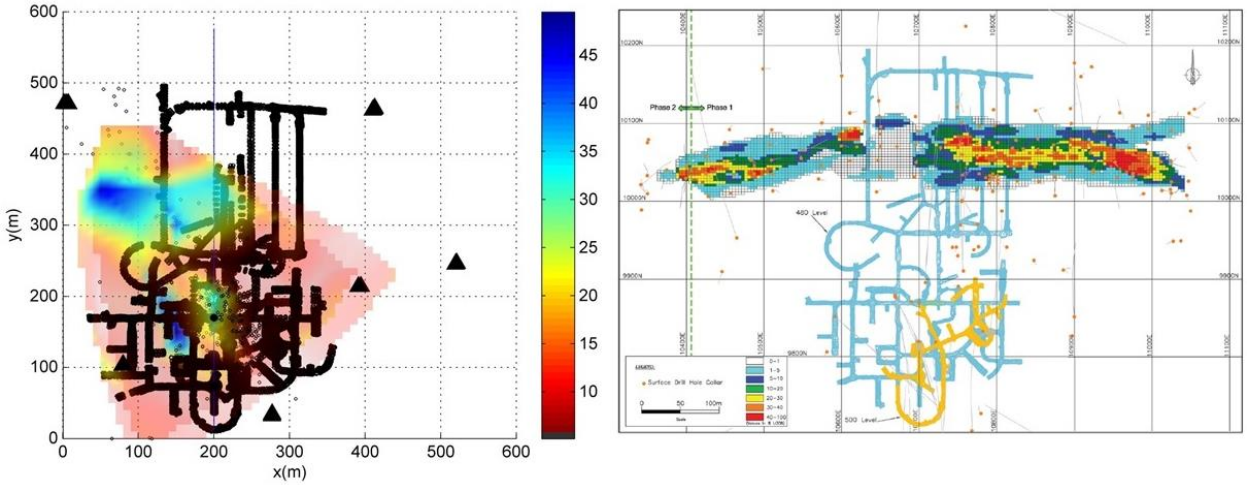

Figure 4: (Left) Same as figure 3 (left) but with Q values between 0-50 and map view at z=400-500 m. The high quality ore deposit part correlates with Q=40-50 and low quality correlates with Q=30-35. (Right) Map view of the Uranium mine cavity grade distribution.

Conclusions

Attenuation tomography with the t* measurements applied to microseismic data has shown to be a promising tool to image and investigate the properties of ore deposits and the region where the seismic cloud is observed. The ore deposits correlate very well with Q values of 30-50 whereas the seismic cloud has lower Q values less than 10. Moreover, the quality of the ore deposit can also be assessed as a slight difference in Q. High quality ore correlates with Q values of 40-50 and low quality with 30. These small differences in Q may not be resolvable with velocity tomography alone. Rather we suggest a joint interpretation of velocity and attenuation tomography for a better understanding of the material properties of the region. The same methodology holds also promise for microseismic data acquired during hydraulic fracturing treatments, where attenuation values may be correlated to fracture densities.

Acknowledgements

The authors thank an anonymous company for permission to use this dataset and the financial support provided by the sponsors of the Microseismic Industry Consortium. We also thank Edouard Kravchinsky and Ibinabo Bestmann for pre-processing of data.

References

Bao, X., Sandvol, E., Ni, J., Hearn, T., Chen, Y. J., & Shen, Y. (2011). High resolution regional seismic attenuation tomography in eastern Tibetan Plateau and adjacent regions. *Geophysical Research Letters*, *38*(16).

Barthwal H. and Van der Baan M. (2014) *Passive seismic tomography using recorded microseismicity.* 84th Ann. Int. Mtg., SEG, Denver.

Calixto, F. J. et al., (2013). Velocity structure beneath the southern Puna plateau: Evidence for delamination. *Geochemistry, Geophysics, Geosystems*, *14*(10), 4292-4305.

Calixto, F. J. et al., (2014). Shear wave splitting and shear wave splitting tomography of the southern Puna plateau. *Geophysical Journal International*, *199*(2), 688-699.

Castellanos F. and Van der Baan M. (2013) *Microseismic event locations using the double-difference algorithm.* CSEG Recorder, 38(3), 26-37.

Castellanos F. and Van der Baan M. (2014) *Dynamic triggering of microseismicity in a mine setting.* 2014 GeoConvention, Calgary.

Der, Z. A., & Lees, A. C. (1985). Methodologies for estimating t*(f) from short-period body waves and regional variations of t*(f) in the United States. *Geophysical Journal International*, *82*(1), 125-140.

Eaton D. W., Van der Baan M., Birkelo B. and Tary J-B. (2014) *Scaling relations and spectral characteristics of tensile microseisms: Evidence for opening/closing cracks during hydraulic fracturing.* Geophysical Journal International, 196(3), 1844-1857.

Herrera R. H., Han J. and M. van der Baan (2014) *Applications of the synchrosqueezing transform in seismic time-frequency analysis.* Geophysics, 79(3), V55-V64.

Preston, L. (2014). *Seismic Attenuation Inversion with t* Using tstarTomog* (No. SAND2014-17970). Sandia National Laboratories (SNL-NM), Albuquerque, NM (United States).

Reine C., Clark R. and Van der Baan M. (2012a) *Robust prestack Q-determination using surface seismic data: I - Method and synthetic examples.* Geophysics, 77 (1), R45-R56.

Tonn, Rainer. "The determination of the seismic quality factor Q from VSP data: a comparison of different computational methods." *Geophysical Prospecting* 39.1 (1991): 1-27.